Neuro-Oncology 12(2):133–144, 2010.
doi:10.1093/neuonc/nop043

Hyperpolarized ^{13}C magnetic resonance metabolic imaging: application to brain tumors

Ilwoo Park, Peder E. Z. Larson, Matthew L. Zierhut, Simon Hu, Robert Bok, Tomoko Ozawa, John Kurhanewicz, Daniel B. Vigneron, Scott R. VandenBerg, C. David James, and Sarah J. Nelson

Joint Graduate Group in Bioengineering, University of California–San Francisco/Berkeley, San Francisco, California (I.P., S.H., J.K., D.B.V., S.J.N.); Surbeck Laboratory of Advanced Imaging, Department of Radiology and Biomedical Imaging, University of California–San Francisco, San Francisco, California (I.P., P.E.Z.L., M.L.Z., S.H., R.B., J.K., D.B.V., S.J.N.); Department of Neurological Surgery, University of California–San Francisco, San Francisco, California (T.O., S.R.V., C.D.J.); Department of Pathology, University of California–San Francisco, San Francisco, California (S.R.V.)

In order to compare in vivo metabolism between malignant gliomas and normal brain, ^{13}C magnetic resonance (MR) spectroscopic imaging data were acquired from rats with human glioblastoma xenografts (U-251 MG and U-87 MG) and normal rats, following injection of hyperpolarized [1-^{13}C]-pyruvate. The median signal-to-noise ratio (SNR) of lactate, pyruvate, and total observed carbon-13 resonances, as well as their relative ratios, were calculated from voxels containing Gadolinium-enhanced tissue in T_1 postcontrast images for rats with tumors and from normal brain tissue for control rats. [1-^{13}C]-labeled pyruvate and its metabolic product, [1-^{13}C]-lactate, demonstrated significantly higher SNR in the tumor compared with normal brain tissue. Statistical tests showed significant differences in all parameters ($P < .0004$) between the malignant glioma tissue and normal brain. The SNR of lactate, pyruvate, and total carbon was observed to be different between the U-251 MG and U-87 MG models, which is consistent with inherent differences in the molecular characteristics of these tumors. These results suggest that hyperpolarized MR metabolic imaging may be valuable for assessing prognosis and monitoring response to therapy for patients with brain tumors.

Received December 16, 2008; accepted March 12, 2009.

Corresponding Author: Ilwoo Park, Joint Graduate Group in Bioengineering, Surbeck Laboratory of Advanced Imaging, University of California–San Francisco/Berkeley, 1700 4th Street, Byers Hall, Room BH-303, San Francisco, CA 94158-2532 (ipark@radiology.ucsf.edu).

Keywords: brain tumor, dynamic nuclear polarization (DNP), human glioblastoma xenograft, hyperpolarized carbon-13 metabolic imaging

It is well known that malignant transformation is associated with increased glycolytic flux and high cellular lactate excretion.[1] Cancers preferentially rely on nonoxidative glycolysis for energy production, and excess lactate is produced as a result. With regard to brain tumors, a number of studies have shown increased lactate production in human glioma[2,3] and in rat glioma models.[4,5] These studies suggest that lactate may be used as a biomarker for both anaerobic glycolysis and reduced cellular oxygenation, and that lactate detection may be important for assessing prognosis and detecting brain tumor response to therapy.

Proton magnetic resonance spectroscopy (^{1}H MRS) has been one of the major tools applied to the noninvasive detection of lactate in brain tumors.[6,7] Several studies have demonstrated the clinical significance of assessing lactate for the management of brain tumor patients using ^{1}H MRS. Sijens et al.[8] and Li et al.[9] showed the association of lactate and lipid signals in ^{1}H magnetic resonance spectroscopic imaging (MRSI) with the diagnosis of high-grade tumors. Saraswathy et al.[10] demonstrated that elevated lactate and lipid signals were associated with poor survival in patients with glioblastoma multiforme (GBM) who were examined prior to radiation and chemotherapy. The interpretation of lactate as measured by ^{1}H MRS remains complex.[11] The steady-state lactate signal that is observed using this methodology may stem from

increased glycolysis in cancerous cells, but also depends on the rate of lactate production and clearance. A further complication is that the observed signal may originate from lactate that is accumulating in cystic or necrotic regions.

In an attempt to overcome these complications, ^{13}C MRS has been used to study in vivo tumor metabolism in the brain tumor model of animals[4,12] and in patients with brain tumors.[13] In these studies, tumor glycolytic metabolism was investigated using ^{13}C MRS after the injection of ^{13}C-labeled glucose. The altered energy metabolism in tumors was confirmed by the elevated production of ^{13}C-labeled lactate in tumor tissue. The intrinsically low concentration of ^{13}C cellular metabolites and the consequently low sensitivity compared with ^{1}H MRS limit the application of this technique in the clinic. Another approach is the use of positron emission tomography (PET) imaging with 2-[^{18}F]fluoro-2-deoxy-D-glucose (FDG), which has been established as a molecular imaging tool for monitoring the uptake of FDG, which is an analog of glucose.[14,15] Despite its high sensitivity and appealing potential to assist in the diagnosis and management of many cancers,[16,17] the low specificity of this technique and the high levels of FDG uptake in normal grey matter have also limited its application in clinical neuro-oncology.

Dynamic nuclear polarization (DNP) and the recent development of a dissolution process that retains polarization into the liquid state enable the real-time investigation of in vivo metabolism with more than 10 000-fold signal increase over conventional ^{13}C methods.[18,19] Previous studies have demonstrated the promise of this technique for examining in vivo tumor metabolism for application in the management of cancer.[20–22] Hyperpolarized ^{13}C-pyruvate, labeled at the C1 position, may be used as a substrate for evaluating metabolism by high-resolution ^{13}C MRSI, which can be integrated with anatomic proton magnetic resonance imaging (MRI). Chen et al.[20] showed elevated [1-^{13}C]-lactate in both primary and metastatic tumors in a transgenic adenocarcinoma of mouse prostate (TRAMP) model, whereas normal prostate tissue produced much less [1-^{13}C]-lactate. To our knowledge, this study demonstrated, for the first time, the use of hyperpolarized 13C agents to study brain tumor metabolism in an in vivo model system. Day et al.[21] demonstrated that the DNP technique can be used to detect tumor response to treatment in lymphoma-bearing mice in vivo. These studies were based on the premise that cancer cells preferentially generate lactic acid for cellular energy production and that pyruvate, which is an end product of glycolysis, is excessively converted to lactate via lactate dehydrogenase (LDH) in tumor tissues.[1,23] The injection of ^{13}C-pyruvate and assessment of ^{13}C-lactate can be used to distinguish cancerous tissue from normal healthy tissue.[22,24]

The purpose of the current study was to explore the feasibility of using ^{13}C MRSI with hyperpolarized [1-^{13}C]-pyruvate as a substrate for evaluation of in vivo tumor metabolism in a rat brain tumor model with a human glioblastoma xenograft, and compare it with normal rat brain. In this study, two human GBM tissue-cultured cell lines were used to generate tumors in the rat brain. These tumor models exhibited distinct heterogeneity in growth characteristics and histology, which simulated some of the characteristics of human GBM.[25] In conducting this study, we characterized and compared ^{13}C imaging parameters with results from immunohistochemical analysis. This study demonstrated, for the first time, to our knowledge, the use of hyperpolarized ^{13}C agents to study brain tumor metabolism in an in vivo model system.

Materials and Methods

Cell Culture and Implantation of Intracerebral Tumors

The details of the cell culture and intracerebral implantation procedures have been described elsewhere.[25,26] In brief, U-251 MG and U-87 MG human GBM cell lines obtained from the Tissue Bank in the Department of Neurological Surgery at the University of California, San Francisco, were maintained as exponentially growing monolayers in complete medium consisting of Eagle's minimal essential medium with 10% fetal calf serum and 1% nonessential amino acids. Cells were cultured at 37°C in a humidified atmosphere consisting of 95% air and 5% CO_2. Cells were harvested by trypsinization, washed once with Hanks' Balanced Salt Solution, and resuspended in Hanks' Balanced Salt Solution for implantation. Five-week-old male athymic rats (rnu/rnu, homozygous) purchased from Harlan (Indianapolis, Indiana) were housed under aseptic conditions with filtered air and sterilized food, water, bedding, and cages. For implantation, rats were anesthetized with an intraperitoneal injection of ketamine (60 mg/kg) and xylazine (7.5 mg/kg). Ten microliters of cell suspension (2×10^6 cells for U-251 MG and 5×10^6 cells for U-87 MG) were slowly injected into the right caudate-putamen of rat brain using an implantable guide-screw system. All protocols for animal studies were approved by the UCSF Institutional Animal Care and Use Committee.

Animal Preparation

Nine male athymic rats (median weight 270 g) with human GBM xenograft tumors (4 arising from U-251 MG cell lines and 5 from U-87 MG cell lines) and 6 normal male Sprague–Dawley rats (median weight 300 g) were included in this study. Owing to the difference in growth characteristics of the 2 cell lines,[25] rats implanted with U-251 MG cell lines were scanned approximately 40 days and those implanted with U-87 MG cell lines were scanned 18 days after tumor implantation (Table 1). Before each imaging experiment, the rat was placed on a heated pad and anesthetized with isoflurane (2%–3%). A catheter was placed into the tail vein for the intravenous administration of hyperpolarized pyruvate solution. The rat was placed on a heated pad positioned in the RF coil in the MR

Table 1. Summary of the rats evaluated in this study

Rat ID	Tumor cell type	Study date from tumor transplantation (days)	Weight (g)	Pyruvate injection volume[a] (mL)	Polarization[a] (%)
Normal 1	N/A	N/A	360	3.3	16.9
Normal 2	N/A	N/A	300	2.7	17.2
Normal 3	N/A	N/A	240	2.3	22.1
Normal 4	N/A	N/A	290	2.3	21.6
Normal 5	N/A	N/A	300	2.3	21.8
Normal 6	N/A	N/A	390	2.6	18.1
Tumor 1	U-251 MG	30	280	2.4	16.7
Tumor 2	U-251 MG	38	270	2.3	19.7
Tumor 3	U-251 MG	41	360	2.2	20.1
Tumor 4	U-251 MG	49	340	2.3	21.3
Tumor 5	U-87 MG	18	260	2.3	17.6
Tumor 6	U-87 MG	20	270	2.3	19.5
Tumor 7	U-87 MG	14	210	2.3	14.9
Tumor 8	U-87 MG	18	220	2.3	16.6
Tumor 9	U-87 MG	21	290	2.3	10.6

N/A, not applicable.
[a]The listed injection volume and polarization are for 2D MRSI study.

scanner. Anesthesia was continued with a constant delivery of isoflurane (1%–2%) through a long tube to a cone placed over the rat's nose and mouth while the rat was in the scanner. The vital signs such as heart rate and oxygen saturation were continuously monitored. The body temperature was maintained at 37°C throughout the imaging procedures by maintaining a flow of heated water through the pad underneath the rat.

Polarization Procedure

A detailed description of the polarization procedure and dissolution process was previously published.[20,27] In brief, a mixture of 32 μL (approximately 40 mg) [1-^{13}C]-pyruvate (Isotec, Miamisburg, Ohio) and 15 mM OX63 trityl radical (Oxford Instruments, Abingdon) was hyperpolarized using a HyperSense® DNP polarizer (Oxford Instruments, Abingdon, UK) in a field of 3.35 T at approximately 1.4 K by irradiation with 94.1 GHz microwaves similar to the previous description.[18] After approximately 60 minutes of microwave irradiation, the hyperpolarized pyruvic acid was rapidly dissolved in a saline solution with 5.96 g/L Tris (40 mM), 4.00 g/L NaOH (100 mM), and 0.1 mg/L Na_2EDTA to produce a 100 mM solution of pyruvate with a liquid-state pH of 7.6. Approximately 2.3 mL of this solution was then injected into the tail vein of a rat within 10 seconds of removal from the polarizer. The injection lasted 12 seconds and was followed by a quick saline flush for both dynamic and spectroscopic imaging studies. Immediately after dissolution, an aliquot of the pyruvate solution was used to measure the liquid-state polarization using an in-house-built low-field NMR spectrometer. Levels of polarization ranged from 11% to 23% (median polarization 18%) (Table 1). The pH of the final solution was also measured (median pH 7.97 ± 0.77).

^{1}H and ^{13}C MR Imaging

Experiments were performed using a 3 T GE Signa™ scanner (GE Healthcare, Milwaukee, Wisconsin) equipped with the multinuclear spectroscopy hardware package. The RF coil used in these experiments was a dual-tuned ^{1}H–^{13}C coil with a quadrature ^{13}C channel and linear ^{1}H channel with an 8 cm inner coil diameter and 9 cm length constructed based on an earlier design.[28]

High-resolution T_2-weighted anatomical images were obtained in all 3 planes using a fast spin-echo (FSE) sequence. Axial images were acquired in 8 minutes with an 8 cm FOV, 320 × 192 matrix, 2 mm slice thickness, and 5 NEX. Sagittal and coronal images were acquired in 6.5 minutes with an 8 cm FOV, 256 × 192 matrix, 2 mm (sagittal) or 1.5 mm (coronal) slice thickness, and 4 NEX.

Dynamic ^{13}C spectroscopic data were acquired from a 15 mm slice through the brain. Spectra were obtained every 3 seconds (TR = 3 seconds) for a period of 3.2 minutes using a double spin-echo pulse sequence consisting of a 5° flip angle RF excitation, 15 mm axial slice thickness, a pair of nonlocalized 180° hyperbolic secant refocusing pulses, TE = 35 ms, 5 kHz spectral bandwidth (BW), and 2048 spectral points.[27,29] Data acquisition started simultaneously with the injection of hyperpolarized [1-^{13}C]-pyruvate and continued until a total of 64 spectra had been acquired in 192 seconds.

The ^{13}C 2-dimensional (2D) MRSI data were acquired using a double spin-echo pulse sequence with a slice-selective variable small flip angle excitation

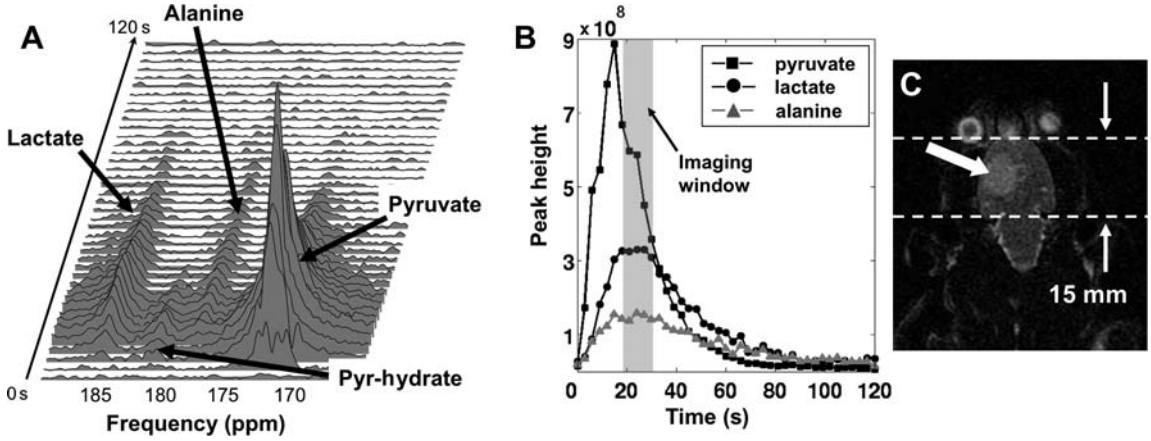

Fig. 1. A representative example of hyperpolarized ^{13}C dynamic data from a rat with tumor (Tumor 6). The stack plot of ^{13}C magnitude spectra (A) and the peak height plots (B) show the time course of the hyperpolarized [1-^{13}C]-pyruvate and its metabolic products after the injection of 2.3 mL hyperpolarized pyruvate. Forty ^{13}C spectra were plotted in the stack plot (A), and the peak heights of pyruvate, lactate, and alanine are plotted for 120 seconds after the injection (B). The pyruvate peak was scaled down by a factor of 2 for viewing purposes in (B). Both data show the hyperpolarized pyruvate quickly reaching its maximum approximately 15 seconds after the injection and its conversion to lactate and alanine. (A) T2 FSE image in the coronal plane (C) shows the hyperintense region inside the brain (arrow), which depicts the extent of tumor. The dashed line indicates the 15 mm slice thickness used for acquiring the ^{13}C dynamic data.

pulse and a pair of nonlocalized 180° hyperbolic secant refocusing pulses.[29] A 12 × 8 phase-encoding matrix and 60 × 40 mm FOV on a 10 mm selected slice gave an in-plane resolution of 5 × 5 mm and 0.25 cm^3 voxel resolution, and was acquired in 11 seconds with TE/TR = 35/110 ms, 5 kHz BW, and 256 spectral points. Based on the changes in metabolite intensity seen from the ^{13}C dynamic data (Fig. 1B), the MRSI acquisition began 20 seconds after the start of the injection. This was designed to obtain the data while the hyperpolarized ^{13}C-lactate was at a maximum. Centric k-space encoding and variable flip angle acquisition schemes were used to enable the efficient use of the hyperpolarized magnetization.[30]

For the rats with tumors, pre- and post-Gadolinium (Gd) T_1-weighted axial anatomical images were obtained using a spin-echo sequence before and after the injection of 0.3 mL Gd-DTPA (approximately 0.3 mmol/kg, diluted 1:2 with saline). These were acquired in 16 minutes with an 8 cm FOV, 320 × 192 matrix, 1.2 mm slice thickness, and 7 NEX.

Immunohistochemical Analysis

For immunohistochemical analysis, the rats with tumors were euthanized after the imaging experiment. Their brains were immediately removed and fixed by immersion in 10% buffered formalin. The fixed brains were then trimmed into multiple coronal sections and subsequently dehydrated by graded ethanols and embedded in wax (Paraplast Plus, McCormick Scientific) using routine techniques. All sections were cut at 5 μm and mounted on *Superfrost/Plus* slides (Fisher Scientific). All coronal sections were examined by H&E staining. Antibodies to the following epitopes were obtained from commercial sources and used at the following dilutions and incubation times/temperatures: (i) carbonic anhydrase 9 (CA9) (#NB 100-417, Novis Biologicals, Littleton Colorado) at 1:500, 32 minutes/37°; and (ii) Ki-67 (MIB-1; anti-Ki-67[30-9], Ventana Medical Systems, Inc., Tucson, Arizona) at 2 μg/mL, 32 minutes/37° after preincubation in 3% H_2O_2/methanol for 16 minutes. Epitope retrieval for all antibodies was performed for 30 minutes in Tris buffer, pH 8, at 90°. All immunohistochemistry was performed on the Ventana Medical Systems Benchmark XT using the iView (Avidin-Biotin) detection system with A-V blocking.

Data Processing

The hyperpolarized ^{13}C dynamic data were processed with MATLAB™ 7.0 (Mathworks Inc., Natick, Massachusetts). Individual FIDs were apodized with a 10 Hz Lorentzian filter in the time domain and Fourier-transformed to produce ^{13}C spectrum at each time point. Using the magnitude spectra, the peak heights of lactate, alanine, and pyruvate were obtained and plotted as a function of time (Fig. 1). The hyperpolarized ^{13}C 2D MRSI data were processed with software developed in our laboratory and that was described previously.[31] The k-space FIDs were apodized by a 16 Hz Gaussian filter in the time domain and zero-filled to 512 points. The data were then Fourier-transformed to produce a 2D array of spectra from different spatial locations.

Data Analysis

In order to analyze ^{13}C metabolic parameters for each study, the signal-to-noise ratio (SNR) of lactate, pyruvate, and total carbon (tC: a sum of lactate, pyruvate–

hydrate, alanine, and pyruvate SNR), and also the ratio of lactate over pyruvate (Lac/Pyr), lactate over total carbon (lac/tC), and pyruvate over total carbon (Pyr/tC) were calculated from the ^{13}C 2D MRSI data using the magnitude spectra. In order to estimate the SNR, the integrals for lactate, pyruvate–hydrate, alanine, and pyruvate were scaled by the standard deviation of the noise estimated from the first 100 points of the spectrum that contained no metabolite resonances. All SNR values were normalized according to polarization (in %) and injection volume (in mL) for each examination by:

$$\text{Normalized SNR} = \text{SNR} \times (18\%/\text{polarization}) \times (2.3\,\text{mL/injection volume}).$$

The carbon spectra were voxel shifted in order to minimize partial volume effects[32] by applying linear phase to the k-space data as described by the Fourier shift theorem.[33] To investigate differences in metabolism between rats with tumors and controls, each ^{13}C parameter was compared between the voxels containing Gd-enhanced brain tissue in the T_1-weighted post-Gd image of the rats with tumors and the normal brain tissue of control rats. Box plots of each parameter were created and compared between the tumor and normal groups. Images of each parameter were generated by spatially interpolating the normalized values of each parameter to the resolution of anatomical images using a linear kernel and overlaying it on the anatomical images. Each ^{13}C imaging parameter was compared between the rats with U-251 MG and U-87 MG tumors to investigate the differences in metabolic imaging markers between the 2 types of tumor.

For immunohistochemical analysis, MIB-1 index (in %), CA-9 index (in %), and percent necrosis were compared between the rats with U-251 MG and U-87 MG tumors. For each tumor type, MIB-1 values were compared with ^{13}C imaging parameters in order to test for correlation between the degree of proliferation and ^{13}C metabolic imaging markers. Mann–Whitney rank-sum test was used for all statistical comparisons, and Spearman rank correlation for the test of correlation.

Results

The use of hyperpolarized [1-^{13}C]-pyruvate provided sufficient signal to detect its transfer of the ^{13}C label to lactate and alanine. Figure 1A shows representative ^{13}C dynamic spectra from a 15 mm slice of rat brain with a tumor. Each horizontal line corresponds to a magnitude spectrum acquired at a time resolution of 3 seconds. From these spectra, the peak height of each metabolite was determined, with values plotted as a function of time (Fig. 1B). Typically, the [1-^{13}C]-pyruvate signal (173 ppm) reached its maximum at approximately 15 seconds after the start of hyperpolarized pyruvate injection, and was followed by the [1-^{13}C]-lactate signal maximum (185 ppm) at approximately 20 seconds following pyruvate injection. After reaching its maximum, the lactate signal maintained a relatively constant level for 10–15 seconds. The pyruvate signal decreased rapidly from its

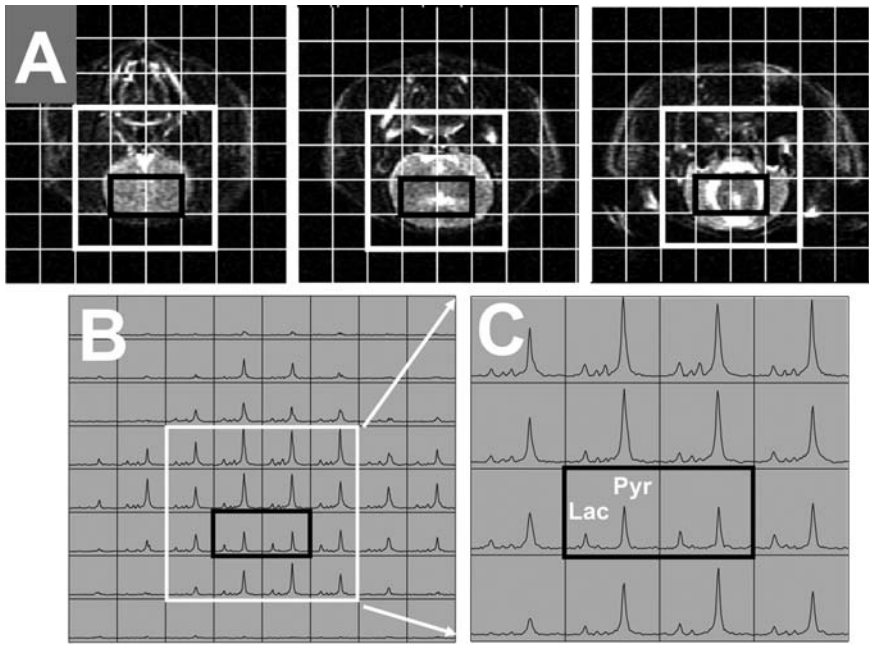

Fig. 2. Representative hyperpolarized ^{13}C 2D MRSI data from a normal rat (Normal 4). The spectral arrays were overlaid on top of axial T2 FSE images at different locations within the ^{13}C MRSI slice (A). The corresponding magnitude spectra (B) and the zoomed-in spectra around the rat brain (C) showed hyperpolarized [1-^{13}C]-pyruvate and its conversion to other metabolites. The normal brain tissues (voxels inside the black box) displayed ample SNR of lactate and pyruvate. The pyruvate signal inside the brain was low compared with that in the other regions outside the brain, presumably due to the intact BBB.

maximum peak, and the lactate signal deceased at a slightly slower rate than the pyruvate. [1-^{13}C]-alanine and pyruvate–hydrate were also observed, but the signal levels were low. Figure 1C contains a T_2-weighted coronal FSE image illustrating the slice coverage of the hyperpolarized ^{13}C dynamic data acquisition. As a result of these observations, the period of 20–35 seconds following injection was used as an imaging window for subsequent ^{13}C 2D MRSI studies.

The ^{13}C 2D MRSI data demonstrated excellent detection of ^{13}C-labeled lactate and pyruvate resonances in both the normal rats and the rats with tumors. The [1-^{13}C]-lactate resonance exhibited significantly higher SNR in the tumor brain tissue compared with the normal brain tissue. The [1-^{13}C]-pyruvate resonance was also observed to be higher in tumors compared with normal brain tissue. The pyruvate–hydrate and alanine signals appeared to be minimal in brain tissue.

Representative hyperpolarized ^{13}C 2D MRSI data of a normal rat are shown in Fig. 2. The spectral array (Fig. 2B) was overlaid on three axial T2 FSE images within the MRSI slice (Fig. 2A). Spectra around the brain are magnified as shown in Fig. 2C, with the black box highlighting voxels inside the brain. The pyruvate peak inside the brain showed an SNR of 99.7 (median, ranged from 71.1 to 119.3), but this was considerably lower compared with the pyruvate peaks in the nonbrain tissue around the brain, suggesting that the amount of pyruvate that passed through the blood brain barrier (BBB) was relatively low. The region outside the brain (voxels above the black box in Fig. 2C) consistently exhibited a high level of pyruvate, which most likely originated from blood vessels, including the internal carotid artery and the vertebrobasilar arterial system that runs in the ventral surface of the brainstem. The lactate peak inside the brain was relatively small compared with the pyruvate peak (Fig. 2C).

Figure 3 shows representative magnitude spectra from hyperpolarized ^{13}C 2D MRSI data and the corresponding anatomical images of rat brains with tumor. The spectral array had a 5 × 5 mm nominal in-plane resolution and 1 cm slice thickness (Fig. 3B) and was overlaid on 3 axial T1 post-Gd images within the ^{13}C MRSI

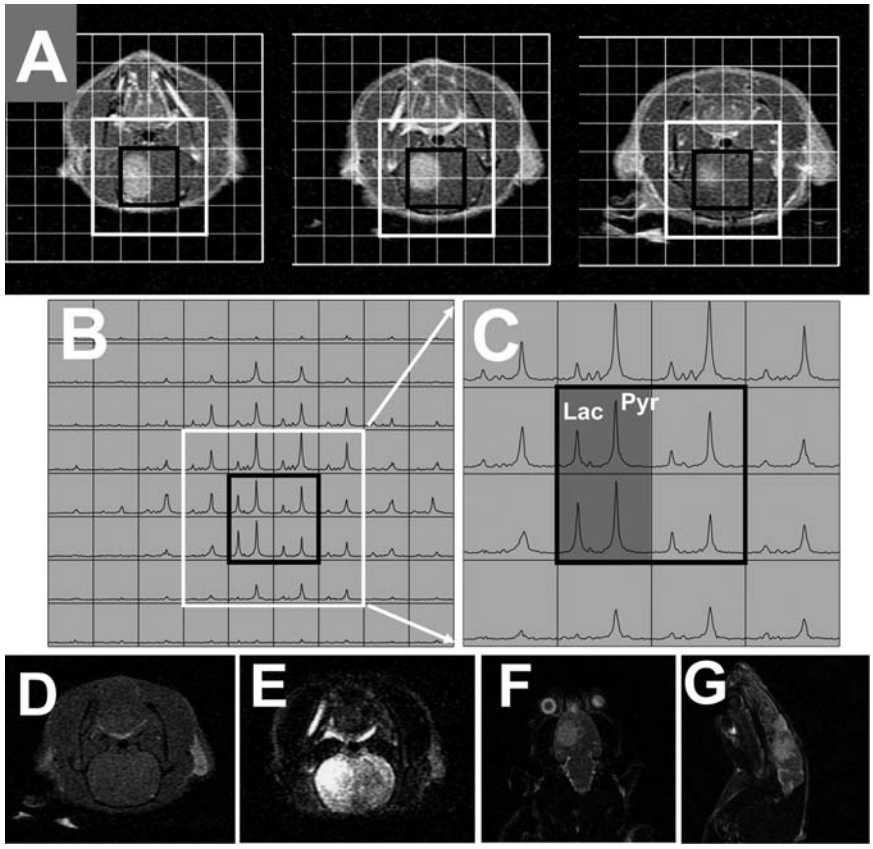

Fig. 3. Representative anatomical images and the corresponding magnitude spectra from a hyperpolarized ^{13}C 2D MRSI study of a rat with tumor (Tumor 6). Axial T1 post-Gd images within the MRSI slice show contrast-enhancing lesion inside the brain (A). These 1.2 mm thick axial images represent a fraction of volume that contributed to the ^{13}C signal acquired from a 10 mm slice. The white and black boxes represent the voxels around the brain and inside the brain, respectively. The corresponding magnitude spectra (B) and the zoomed-in spectra around the brain (C) clearly showed elevated ^{13}C lactate and pyruvate levels in the tumor (highlighted voxels in the black box in C) compared with the brain tissue in the contra-lateral hemisphere and, most importantly, the brain tissue from the normal rats (Fig. 2C). An axial T_1 pre-Gd image (D) and T_2 FSE images in axial, coronal, and sagittal planes (E–G) are also shown.

slice (Fig. 3A). A contrast-enhancing lesion is seen in an axial T1 post-Gd image, and marks the boundary of tumor tissue whose BBB is disrupted. The white box in the T1 post-Gd images (Fig. 3A) and the corresponding magnitude spectra (Fig. 3B) represent zoomed-in regions around the rat brain. The voxels inside the brain are highlighted with a black box (Fig. 3C). The 2 highlighted voxels in the left column of the black box are from the contrast-enhancing lesion of the rat brain, and exhibit highly elevated lactate compared with the tissue in the contra-lateral hemisphere, other tissues around the brain, and most importantly the brain tissue from normal rats (Fig. 2C). The level of pyruvate was higher in the tumor region compared with brain tissue from the contra-lateral hemisphere and other tissues around the brain and the brain of rats without tumor. Axial T1 pre-Gd image and T2 FSE images in axial, coronal, and sagittal planes are also shown in Fig. 3D–G. The hyperintense region in the T2 FSE images illustrates the extent of the tumor and corresponds to the location of the contrast-enhancing lesion in the T1 post-Gd images.

Quantification of the hyperpolarized ^{13}C 2D MRSI data is depicted in Fig. 4. The SNR of lactate, pyruvate, and total carbon as well as their relative ratios (Lac/Pyr, Lac/tC, and Pyr/tC) demonstrated major differences in ^{13}C metabolic profiles between the rats with tumors and control rats. All 6 ^{13}C imaging parameters were significantly different between rats with and without tumor ($P < .0004$). Representative maps of each ^{13}C parameter are shown for a rat with tumor and normal rat in Fig. 5. The ^{13}C metabolite images were generated by interpolating the values of each parameter to the resolution of the axial T1 post-Gd image for the rat with tumor and the axial T1 pre-Gd image for the normal rat. The interpolated values from the rat with tumor and normal rat were overlaid onto the corresponding anatomical images. The rat with a brain tumor showed high lactate, pyruvate, total carbon, Lac/Pyr, and Lac/tC in the contrast-enhancing lesion, whereas the rat without a tumor had significantly lower levels of these parameters in its brain tissue. The contrast-enhanced brain tissue of the rat with a tumor exhibited lower Pyr/tC than the brain tissue of the normal rat.

In addition to the differences between the brains of rats with and without tumors (Figs. 2–5), ^{13}C metabolic imaging parameters demonstrated distinctive characteristics between the brains of rats with U-251 MG and U-87 MG tumors (Fig. 6). The U-87 MG tumors had significantly higher SNR of lactate,

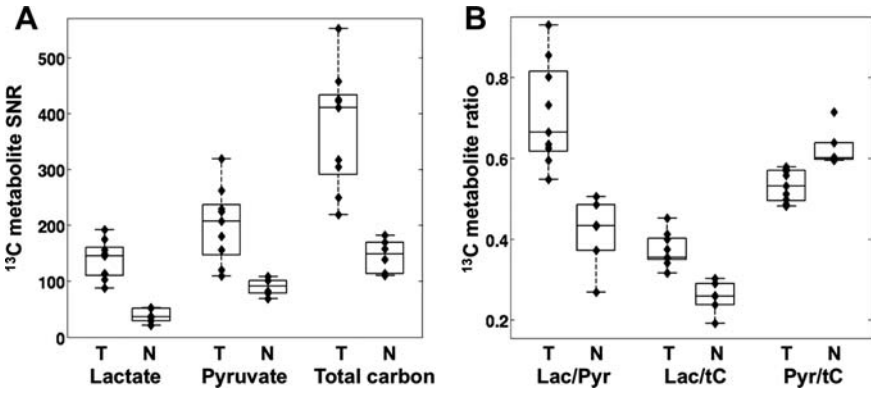

Fig. 4. Comparison of the SNR of lactate, pyruvate, and total carbon (A) and the ratio of Lac/Pyr, Lac/tC, and Pyr/tC (B) between the tumor (T) and normal (N) rats. All ^{13}C parameters showed significant differences and clear separation between 2 groups ($P < .0004$).

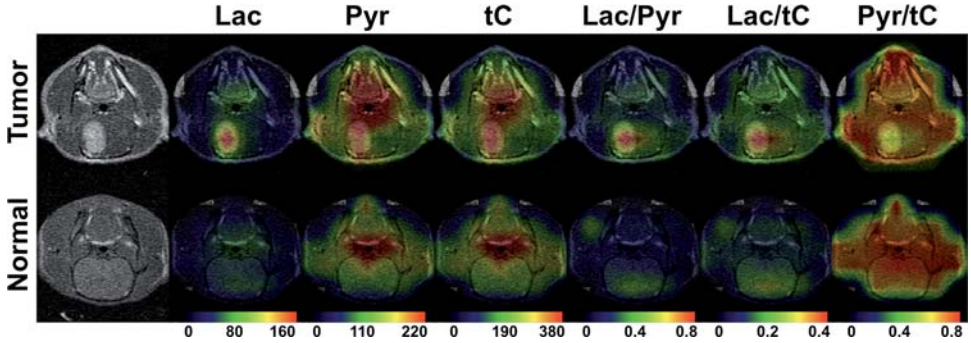

Fig. 5. Metabolic maps of ^{13}C imaging parameters between a rat with tumor and a control rat. All 6 parameters exhibited considerably different intensity between the contrast-enhanced brain tissue of the rat with tumor and the brain tissue of the control rat. Lac, lactate SNR; Pyr, pyruvate SNR; tC, total carbon SNR; Lac/Pyr, lactate over pyruvate ratio; Lac/tC, lactate over total carbon ratio; Pyr/tC, pyruvate over total carbon ratio.

pyruvate, and total carbon than U-251 MG tumors without any overlap of data ($P < .02$). The 2 tumor lines had distinct histopathologic features. With H&E staining, all U-251 MG xenografts had >25% necrosis on any section and this was present in a conspicuous pattern of scattered zones of geographic necrosis (Fig. 7C). In contrast, H&E sections of the U-87 MG xenografts did not demonstrate any significant necrosis and were devoid of the zonal patterns of U-251 MG xenografts (Fig. 7F). The results from immunohistochemical analysis (Table 2) also confirmed that there were distinctive patterns between the 2 tumor types. The CA-9 immunoreactive areas in sections of U-251 MG xenografts, as indicative of cellular hypoxia,[34] were 10%–25% for 3 rats and >25% for the fourth.

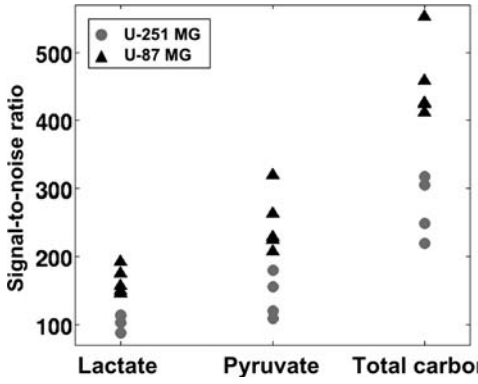

Fig. 6. Comparison of the SNR of lactate, pyruvate, and total carbon between U-251 MG and U-87 MG xenograft. All 3 parameters were significantly different between the 2 tumor types ($P < .02$).

The cellular hypoxia in U-251 MG tumors was distributed in zones (arrow in Figure 7B), which often corresponded to the zones of lower proliferation indicated in MIB-1 staining (arrow in Fig. 7A). In contrast to U-251 xenografts, all of the U-87 xenografts had very low or no CA-9 labeling (Table 2), and did not exhibit zonal MIB-1 labeling (Fig. 7D–E). The percentage of necrosis was significantly different between U-251 MG and U-87 MG tumors ($P < .02$), and there was a strong trend toward difference ($P = .06$) in the CA-9 index (%) between these 2 tumor types. There appeared to be strong correlations between MIB-1 index (%) and the SNR of lactate for each type of tumor ($r = 0.8$) and the SNR of total carbon for U-87 MG tumors ($r = 0.7$), but the statistical significance of this relationship was limited by the relatively small sample size (Fig. 8).

Discussion

This study demonstrated the feasibility of detecting variations in the levels of pyruvate and lactate in human glioblastoma orthotopic xenografts using hyperpolarized [1-^{13}C]-pyruvate as a substrate. The hyperpolarized ^{13}C 2D MRSI data had a nominal spatial resolution of 0.25 cm^3 and demonstrated significant differences in ^{13}C metabolic profiles between tumors and normal brain tissues. The ^{13}C lactate and pyruvate levels in the contrast-enhancing lesions of the brain in rats with tumors were much higher than those in the brains of rats without tumors.

All 6 of the ^{13}C imaging parameters that were evaluated exhibited substantial differences between brains with and without tumors (Fig. 4). The SNR of lactate,

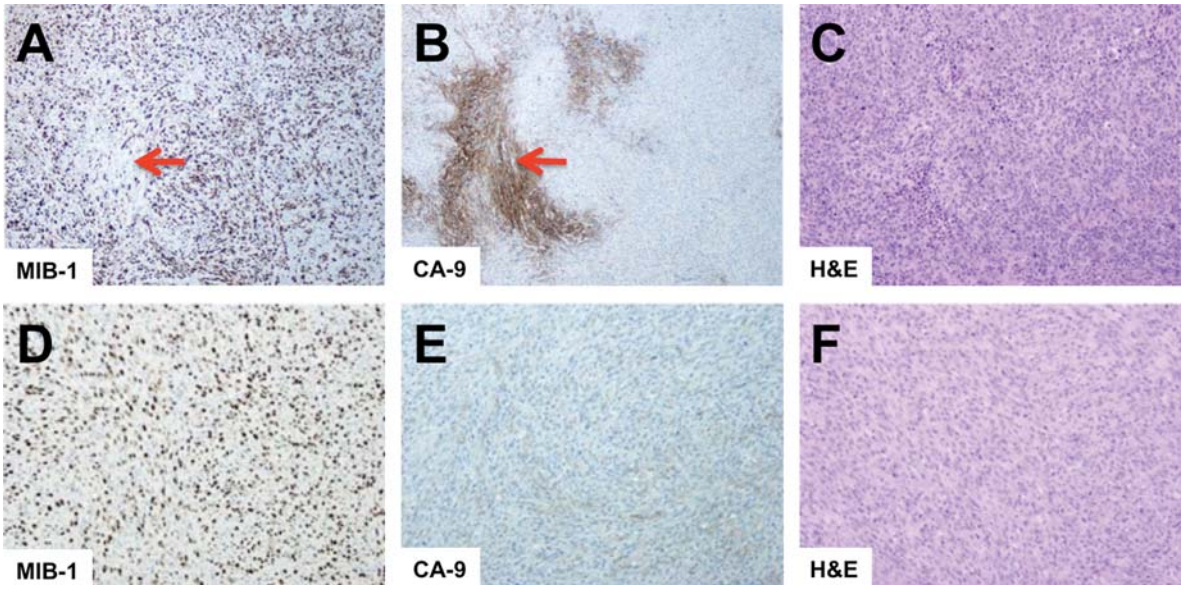

Fig. 7. Staining of U-251 MG (A–C) and U-87 MG (D–F) xenograft with MIB-1 (A, D), CA-9 (B, E), and H&E (C, F). In the U-251 MG tissue, the zones of cellular hypoxia (arrow in B) corresponded to the zones of lower MIB-1 labeling (arrow in A). In contrast to U-251 MG, the U-87 MG xenografts did not exhibit zonal hypoxia or MIB-1 labeling, and there were no large zones of geographic necrosis. All images are at the same magnification.

Table 2. Immunohistochemical evaluation of the rats with intracranial human xenograft tumors

Rat ID	Tumor model	MIB-1 (%)	CA-9 (%)	Necrosis (%)
Tumor 1	U-251 MG	45.65	10–25	≥25
Tumor 2	U-251 MG	57.00	10–25	≥25
Tumor 3	U-251 MG	39.47	10–25	≥25
Tumor 4	U-251 MG	48.11	≥25	≥25
Tumor 5	U-87 MG	39.78	0–10	None
Tumor 6	U-87 MG	43.65	0–10	None
Tumor 7	U-87 MG	48.52	None	0–10
Tumor 8	U-87 MG	37.32	0–10	None
Tumor 9	U-87 MG	40.04	10–25	None

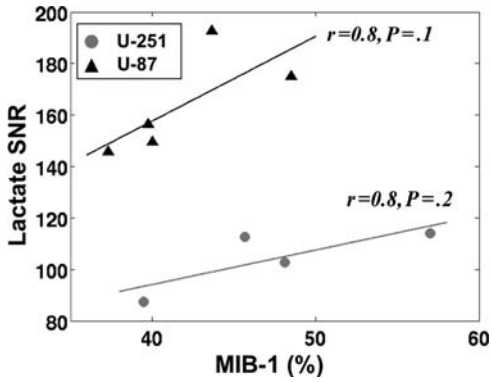

Fig. 8. Correlation between proliferation marker (MIB-1) and the SNR of lactate. Both U-251 MG and U-87 MG tumors showed a strong correlation with MIB-1 index ($r = 0.08$).

pyruvate, and total carbon, and the ratio of Lac/Pyr, Lac/tC, and Pyr/tC, were well separated without any overlap of the data between the 2 groups ($P < .0004$). The substantial differences between ^{13}C cellular metabolism measurements in tumors and normal brains suggest that this method has great potential for monitoring the abnormal metabolism in brain tumors.

Elevated levels of lactate, lactate to pyruvate ratios, and lactate to total carbon ratios are consistent with the findings in previous studies that examined hyperpolarized ^{13}C-labeled lactate in TRAMP mice[20,22] and mouse lymphomas.[21] These studies suggested that hyperpolarized ^{13}C-labled lactate may provide an indirect method for assessing LDH activity. LDH is the enzyme catalyzing the conversion from pyruvate to lactate in glycolysis, which has been seen to have increased activity in brain tumors.[35] A recent study demonstrated that the degree of upregulation correlated with the levels of hyperpolarized ^{13}C-labeled lactate in prostate cancer cell lines.[36] Future studies will examine hyperpolarized ^{13}C metabolites in an ex vivo model of rat brain tumors and compare them with an assay of LDH activity.

U-251 MG and U-87 MG xenografts are well-established cell lines widely used for preclinical studies of brain tumors. Previous studies have shown that there are distinct differences in the histopathologic features of these 2 tumor types.[25,26] U-251 MG tumors consist of a mixture of malignant spindle and epithelioid cells, and contain a large area of necrosis and an irregular border with adjacent brain tissue. U-87 MG tumors are relatively well circumscribed with malignant spindle cells in compact fascicles, and exhibit little or no necrosis. U-251 MG cells also contain more hypoxia than U-87 MG cells.[37] The immunohistochemical data in our study were consistent with these findings (Table 2). The U-251 MG model exhibited large areas of necrosis and hypoxia, whereas the U-87 MG model showed little or no necrosis and hypoxia (Fig. 7). The patterns of contrast enhancement in T1 post-Gd images of rats with U-251 MG and U-87 MG xenografts also indicated that there were marked differences between these 2 tumor types (Fig. 9). The U-87 MG tumors had homogenous levels of contrast enhancement with a well-delineated tumor margin, whereas the U-251 MG tumors exhibited varying levels of contrast enhancement with an irregular tumor margin.

The SNR of lactate, pyruvate, and total carbon of U-87 MG tumors was significantly higher than those of U-251 MG tumors ($P < .02$). The variation in these metabolic profiles may be due to, in part, higher necrotic fraction and thus a relatively smaller number of viable tumor cells in U-251 MG compared with U-87 MG tumors. The higher pyruvate uptake in U-87 MG tumors is consistent with a previous study that showed higher mRNA expression in epithelial tumor cell lines of a monocarboxylate transporter, which has a high

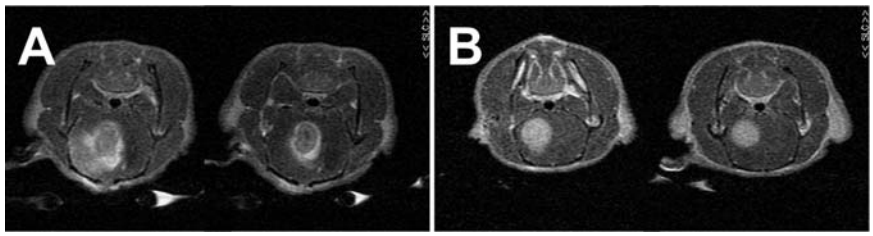

Fig. 9. The patterns of contrast enhancement in T_1 post-Gd images between rats with U-251 MG model (A) and U-87 MG model (B). The U-251 MG tumor displayed heterogeneous levels of contrast enhancement, whereas the levels of contrast enhancement of the U-87 tumor were relatively constant, with well-demarcated tumor margin. The difference in contrast-enhancing patterns may be indicative of inherent differences in molecular characteristics between these 2 tumor models.

Table 3. Comparison of biological, immunohistochemical, and MR features between U-251 MG and U-87 MG model

Type of feature	U-251 MG	U-87 MG
Biological	A mixture of malignant spindle and epithelioid cells with irregular borders	Malignant cells in compact fascicles, with well-circumscribed borders
Histological and immunohistochemical	Larger area of necrosis and hypoxia	Little or no necrosis and hypoxia
MRI	Varying levels of contrast enhancement with an irregular tumor margin	Homogeneous levels of contrast enhancement with a well-delineated tumor margin
^{13}C MRSI	Relatively high SNR of lactate, pyruvate, and total carbon	Relatively low SNR of lactate, pyruvate, and total carbon

affinity for the transport of pyruvate.[38] In addition, low perfusion in necrotic areas of the tumors may result in inadequate delivery of pyruvate to tumor cells. Similarly, the SNR of total carbon, which can be considered as an estimate of the hyperpolarized compounds taken up by the tissue, was in agreement with the difference in necrotic fraction found between U-251 MG and U-87 MG tumors. The differences in ^{13}C metabolic imaging profiles between U-251 MG and U-87 MG models are consistent with the known differences in molecular characteristics between these tumors and suggest that hyperpolarized ^{13}C MRSI that uses pyruvate as a substrate may be useful in characterizing tumor tissues. The different features of U-87 MG and U-251 MG tumors found from this study are summarized in Table 3 and compared with biological characteristics of the 2 tumor models.

Uncontrolled proliferation is one of the major properties of cancer cells. In gliomas, a number of previous studies have correlated proliferation markers with clinical outcome and have validated the MIB-1/Ki-67 index as one of the major predictors of patient survival.[39,40] The strong correlation between the MIB-1 index and the level of ^{13}C-labeled lactate that is converted from hyperpolarized ^{13}C-labeled pyruvate suggests that this methodology may provide an indirect method for characterizing tumor activity and be a potential surrogate marker for prognosis.

Although several imaging techniques such as ^{1}H MRSI, ^{13}C MRS, and PET using FDG as substrate have been applied to evaluate in vivo tumor metabolism,[4–7,12–17] MR metabolic imaging using hyperpolarized ^{13}C substrates has several advantages. With the increase in sensitivity of these ^{13}C substrates, the detection of metabolites is possible at high spatial resolution (0.25 cm^3) in a very short acquisition time (11 seconds). These provide critical improvements over conventional ^{13}C MRS, which is limited by low sensitivity and prohibitively long acquisition time. Unlike ^{1}H MRSI, where the overlapping lipid peaks provide a technical challenge for quantifying lactate, the spectrum obtained using hyperpolarized ^{13}C metabolic imaging lacks a background signal. More importantly, while the interpretation of the steady-state ^{1}H lactate signal is complicated due to the various potential sources of ^{1}H lactate,[11] the lactate signal using ^{13}C MRS reflects only the metabolically active lactate that is generated from hyperpolarized ^{13}C-labeled pyruvate via LDH activity during the experiment. The high reproducibility in the difference in lactate uptake between the tumor and normal brain tissue suggests that this technique will be valuable in assessing prognosis and monitoring brain tumors' response to therapy.

Although the dynamic hyperpolarized ^{13}C data contain important biological information, the results of these studies were primarily used to determine the timing of subsequent 2D MRSI exams. They were limited by the 15 mm-thick slice, which included contributions from the brain, muscle, and vasculature (Fig. 1C). The application of a time-resolved MRSI method with an appropriate spatial resolution[20,41] may be expected to provide more specific information about the dynamics of tumor and normal brain tissue. It should be noted that despite the presence of the BBB, the hyperpolarized ^{13}C 2D MRSI data provided ample SNR for evaluating lactate and pyruvate in both normal brain and tumors (Fig. 4). The high SNR means that it may be possible to obtain an increased coverage with higher spatial resolution in future experiments, and that the application of a fast acquisition technique incorporating a flyback echo-planar readout[20,29] could allow the acquisition of 3D MRSI data that would cover the entire rat brain in a scan time of 10–17 seconds.

The brain tissue in normal rats demonstrated much lower pyruvate and lactate uptake compared with the malignant tumor tissue (Figs. 2C and 3C). The low uptake of pyruvate in the normal brain tissue is thought to be due to the selective permeability of the BBB. It is known that lipid-soluble molecules readily penetrate the BBB whereas charged molecules, which are not lipid-soluble, cross the BBB slowly, or not at all.[42] Since pyruvate is a negatively charged molecule in solution, the crossing of pyruvate molecules through the BBB is restricted. It is impossible to determine the degree of pyruvate signal contribution between the brain tissue and the blood vessels in this study because some of the pyruvate and lactate signal in the brain may come from the capillaries in the endothelial cells of the brain. However, the hyperpolarized lactate-to-pyruvate ratio in normal brain tissue was found to be notably different from that in the voxels located around blood vessels (Fig. 2). In addition, the fact that the rats with U-87 MG and U-251 MG tumors exhibited dissimilar metabolic profiles (Fig. 6)

suggests that the pyruvate was delivered and metabolized in the tumor tissue and the conversion of pyruvate to lactate before its delivery to the tumor tissue was not the major source of the observed hyperpolarized signals. The results from this study suggest that hyperpolarized ^{13}C MRSI is capable of discriminating cancerous and normal brain tissues.

Conclusions

This study demonstrated, for the first time, the feasibility of using the DNP to generate hyperpolarized [1-^{13}C]-pyruvate for evaluating the in vivo metabolism of an orthotopic human glioblastoma xenograft in rat brain. Distinct ^{13}C metabolic characteristics were observed in hyperpolarized ^{13}C MRSI data between the abnormal brain tissue of the rats with tumors and the normal brain tissue of rats without tumors. Moreover, the SNR of lactate, pyruvate, and total carbon were observed to be different between the U-251 MG and U-87 MG models, in a manner that was consistent with inherent differences found from immunohistochemical analysis. This study showed that tumor metabolism in brain tumor models can be examined using hyperpolarized ^{13}C MRSI and suggested that this technique may be useful in assessing prognosis and in monitoring brain tumor response to therapy in patients.

Acknowledgment

The authors would like to thank Vicki Zhang for assistance with the experiments.

Conflict of interest statement. None declared.

Funding

The authors acknowledge research funding support from GE Healthcare and the UC Discovery program, grant ITL-BIO-08-104, and National Institutes of Health grant R01 EB007588.

References

1. Warburg O. On the origin of cancer cells. *Science*. 1956;123(3191):309–314.
2. Kaibara T, Tyson RL, Sutherland GR. Human cerebral neoplasms studied using MR spectroscopy: a review. *Biochem Cell Biol*. 1998;76(2–3):477–486.
3. Herholz K, Heindel W, Luyten PR, et al. In vivo imaging of glucose consumption and lactate concentration in human gliomas. *Ann Neurol*. 1992;31(3):319–327.
4. Terpstra M, Gruetter R, High WB, et al. Lactate turnover in rat glioma measured by in vivo nuclear magnetic resonance spectroscopy. *Cancer Res*. 1998;58(22):5083–5088.
5. Ziegler A, von Kienlin M, Decorps M, Remy C. High glycolytic activity in rat glioma demonstrated in vivo by correlation peak ^{1}H magnetic resonance imaging. *Cancer Res*. 2001;61(14):5595–5600.
6. He Q, Bhujwalla ZM, Glickson JD. Proton detection of choline and lactate in EMT6 tumors by spin-echo-enhanced selective multiple-quantum-coherence transfer. *J Magn Reson B*. 1996;112(1):18–25.
7. Star-Lack J, Spielman D, Adalsteinsson E, Kurhanewicz J, Terris DJ, Vigneron DB. In vivo lactate editing with simultaneous detection of choline, creatine, NAA, and lipid singlets at 1.5 T using PRESS excitation with applications to the study of brain and head and neck tumors. *J Magn Reson*. 1998;133(2):243–254.
8. Sijens PE, Levendag PC, Vecht CJ, van Dijk P, Oudkerk M. 1H MR spectroscopy detection of lipids and lactate in metastatic brain tumors. *NMR Biomed*. 1996;9(2):65–71.
9. Li X, Vigneron DB, Cha S, et al. Relationship of MR-derived lactate, mobile lipids, and relative blood volume for gliomas in vivo. *AJNR Am J Neuroradiol*. 2005;26(4):760–769.
10. Saraswathy S, Crawford FW, Lamborn KR, et al. Evaluation of MR markers that predict survival in patients with newly diagnosed GBM prior to adjuvant therapy. *J Neurooncol*. 2009;91(1):69–81.
11. Kugel H, Heindel W, Ernestus RI, Bunke J, Dumesnil R, Friedmann G. Human brain-tumors—spectral patterns detected with localized H-1 MR spectroscopy. *Radiology*. 1992;183(3):701–709.
12. Ross BD, Higgins RJ, Boggan JE, Willis JA, Knittel B, Unger SW. Carbohydrate metabolism of the rat C6 glioma. An in vivo ^{13}C and in vitro ^{1}H magnetic resonance spectroscopy study. *NMR Biomed*. 1988;1(1):20–26.
13. Wijnen J, Klomp DW, Idema AJ, Galan BE, Heerschap A. (2008) Lactate production in human brain tumor; detection by ^{13}C MRS at 3 T [abstract]. *Proc Intl Soc Mag Reson Med*. 2815.
14. Gambhir SS. Molecular imaging of cancer with positron emission tomography. *Nat Rev Cancer*. 2002;2(9):683–693.
15. Juweid ME, Cheson BD. Positron-emission tomography and assessment of cancer therapy. *N Engl J Med*. 2006;354(5):496–507.
16. Heron DE, Andrade RS, Beriwal S, Smith RP. PET-CT in radiation oncology: the impact on diagnosis, treatment planning, and assessment of treatment response. *Am J Clin Oncol*. 2008;31(4):352–362.
17. Facey K, Bradbury I, Laking G, Payne E. Overview of the clinical effectiveness of positron emission tomography imaging in selected cancers. *Health Technol Assess*. 2007;11(44):iii–iv, xi–267.
18. Ardenkjaer-Larsen JH, Fridlund B, Gram A, et al. Increase in signal-to-noise ratio of >10,000 times in liquid-state NMR. *Proc Natl Acad Sci USA*. 2003;100(18):10158–10163.
19. Golman K, Ardenkjaer-Larsen JH, Petersson JS, Mansson S, Leunbach I. Molecular imaging with endogenous substances. *Proc Natl Acad Sci USA*. 2003;100(18):10435–10439.
20. Chen AP, Albers MJ, Cunningham CH, et al. Hyperpolarized C-13 spectroscopic imaging of the TRAMP mouse at 3 T-initial experience. *Magn Reson Med*. 2007;58(6):1099–1106.
21. Day SE, Kettunen MI, Gallagher FA, et al. Detecting tumor response to treatment using hyperpolarized 13C magnetic resonance imaging and spectroscopy. *Nat Med*. 2007;13(11):1382–1387.
22. Albers MJ, Bok R, Chen AP, et al. Hyperpolarized 13C lactate, pyruvate, and alanine: noninvasive biomarkers for prostate cancer detection and grading. *Cancer Res*. 2008;68(20):8607–8615.
23. Lu H, Forbes RA, Verma A. Hypoxia-inducible factor 1 activation by aerobic glycolysis implicates the Warburg effect in carcinogenesis. *J Biol Chem*. 2002;277(26):23111–23115.

24. Golman K, Zandt RI, Lerche M, Pehrson R, Ardenkjaer-Larsen JH. Metabolic imaging by hyperpolarized ^{13}C magnetic resonance imaging for in vivo tumor diagnosis. *Cancer Res*. 2006;66(22):10855–10860.
25. Ozawa T, Wang JL, Hu LJ, Bollen AW, Lamborn KR, Deen DF. Growth of human glioblastomas as xenografts in the brains of athymic rats. *In Vivo*. 2002;16(1):55–60.
26. Ozawa T, Faddegon BA, Hu LJ, Bollen AW, Lamborn KR, Deen DF. Response of intracerebral human glioblastoma xenografts to multifraction radiation exposures. *Int J Radiat Oncol Biol Phys*. 2006; 66(1):263–270.
27. Kohler SJ, Yen Y, Wolber J, et al. In vivo 13-carbon metabolic imaging at 3 T with hyperpolarized ^{13}C-1-pyruvate. *Magn Reson Med*. 2007;58(1):65–69.
28. Derby K, Tropp J, Hawryszko C. Design and evaluation of a novel dual-tuned resonator for spectroscopic imaging. *J Magn Reson*. 1990;86:645–651.
29. Cunningham CH, Chen AP, Albers MJ, et al. Double spin-echo sequence for rapid spectroscopic imaging of hyperpolarized ^{13}C. *J Magn Reson*. 2007;187(2):357–362.
30. Zhao L, Mulkern R, Tseng CH, et al. Gradient-echo imaging considerations for hyperpolarized ^{129}Xe MR. *J Magn Reson B*. 1996;113(2):179–183.
31. Nelson SJ. Analysis of volume MRI and MR spectroscopic imaging data for the evaluation of patients with brain tumors. *Magn Reson Med*. 2001;46(2):228–239.
32. Vigneron DB, Nelson SJ, Murphy-Boesch J, et al. Chemical shift imaging of human brain: axial, sagittal, and coronal P-31 metabolite images. *Radiology*. 1990;177(3):643–649.
33. Bracewell RN. *The Fourier Transform and Its Applications*. New York: McGraw-Hill; 1978.
34. Yoo H, Baia GS, Smith JS, et al. Expression of the hypoxia marker carbonic anhydrase 9 is associated with anaplastic phenotypes in meningiomas. *Clin Cancer Res*. 2007;13(1):68–75.
35. Subhash MN, Rao BS, Shankar SK. Changes in lactate dehydrogenase isoenzyme pattern in patients with tumors of the central nervous system. *Neurochem Int*. 1993;22(2):121–124.
36. Gisselsson A, Lerche M. (2008) Metabolic activity of diseased and healthy prostate cells investigated as lactate formation from hyperpolarized ^{13}C-pyruvatem [abstract]. *Proc Intl Soc Mag Reson Med*. 251.
37. Wang J, Klem J, Wyrick JB, et al. Detection of hypoxia in human brain tumor xenografts using a modified comet assay. *Neoplasia*. 2003;5(4):288–296.
38. Lin RY, Vera JC, Chaganti RS, Golde DW. Human monocarboxylate transporter 2 (MCT2) is a high affinity pyruvate transporter. *J Biol Chem*. 1998;273(44):28959–28965.
39. Grzybicki DM, Moore SA. Implications of prognostic markers in brain tumors. *Clin Lab Med*. 1999;19(4):833–847.
40. Reavey-Cantwell JF, Haroun RI, Zahurak M, et al. The prognostic value of tumor markers in patients with glioblastoma multiforme: analysis of 32 patients and review of the literature. *J Neurooncol*. 2001; 55(3):195–204.
41. Larson PE, Kerr AB, Chen AP, et al. Multiband excitation pulses for hyperpolarized 13C dynamic chemical-shift imaging. *J Magn Reson*. 2008;194(1):121–127.
42. Davson H, Zlokovic B, Rakic L, Sega MB. An Introduction to the Blood-Brain Barrier. Boca Raton: CRC Press; 1993.